Analysis on 3D fretting contact stresses along thickness under fatigue load

Danilo R.S. Resende[1*], Thiago Doca[1], José A. Araújo[1]

[1]*Dept. of Mechanical Engineering, University of Brasília*
UnB – Faculdade de tecnologia, 70297-400, Brasília - DF, Brazil
** resende.danilo@aluno.unb.br, danilo.rsr98@gmail.com*

Abstract. This work aims to analyse the effect of filleted edges in the stress distribution on a 3D cylinder-plane fretting fatigue problem. The 3D configuration is required since the stresses are distributed along the thickness of the contact interface differently from the common analytical 2D contact stresses solution which consider the plane-strain state to be critical. More recent studies showed results of 3D numerical simulations for different configurations of pad and specimen, but they did not consider the effect of the fatigue load. Herein, focus is given to specimen and pad with the same thickness and both having a small fillet at their edges. This geometry represents well the milling process when fabricating the test specimens employed in fretting fatigue tests. The effect on the filleted edge of each one of the three loads (i.e., contact pressure, fretting load, and fatigue load) are analysed and discussed.

Keywords: Fretting fatigue, 3D numerical fretting, Contact stress

1 Introduction

Fretting is a failure phenomenon that happens when there is contact and a tangential displacement/force between two components. The pressure distribution along the contact is not homogeneous, creating in the contact surface two regions, one of adhesion and other of slip. This partial slip induces differential displacement between the surfaces resulting in high contact stress and strain, which may nucleate a crack. When also under a bulk fatigue load, this crack can grow and generate what is known as fretting fatigue [1].

The relevance of fretting fatigues comes from a considerable number of engineering applications in which mechanical couplings can suffer of this phenomenon such as riveted and bolted joints, dove-tail connections between blades and disc in turbines, in shaft interference and hub connections [2].

Cattaneo-Mindlin [3, 4] were able to calculate the surface stress field, while Hills and Nowell [1] published a well-known 2D approach calculating the stress below contact surface and it has been and still is used in a variety of studies that may result in good estimates of stress gradient, non-linear stress, and life estimates [5, 6]. These calculations consider the plane-strain state as the critical one, in the middle plane of the contact. It is important to emphasize that those methods are capable to provide good estimations, as seen in Rangel et al [7]. Nonetheless, along with the improvement in numerical simulations and computing power, Vázquez et. al [8] demonstrated that life predictions can show non-negligible difference between 2D and 3D approaches. More recently, Vázquez et. al [9] also published a study with a 3D cylinder-flat model includes the thickness relation differences in some common geometries, but does not account for the fatigue bulk load.

In this work, an extension of Vázquez, et al [9] is presented where the effects of the fatigue load are considered. A numerical model is developed using the commercial Finite Element method (FEM) solver ABAQUS. Here, focus is given to a contact configuration where specimen and pad have the same thickness and a small edge fillet is introduced to account for the milling process. The presence of this edge fillet is relevant due to the fact that, in reality, perfectly sharp edges are not possible.

2 Methodology

The methodology procedure was made following six steps. The first step consisted in defining the geometry for the problem, followed by the boundary conditions step. In third place, the contact interaction and properties

were imposed to the problem. In fourth place, it was made the partitioning for a good mesh quality and defining the submodel region. The material properties were also defined as for a simple elastic problem. Lastly, the application of the incremental loads is defined. The detailed description of these steps is given in the following.

2.1 Geometry

The geometry is presented as a group composed by a curved face pad and a dog-bone specimen for fretting fatigue. The simplified problem geometries are depicted in Figure 1. Most of the dimensions are given in terms of the semi-length of the contact zone, a. A good approximation of a is about 1.5-2.0 mm. The problem is solved as a full 3D configuration. This three-dimensional solution aims to compare the contact pressure and shear stress along the thickness of the specimen with the analytical plane-strain 2D contact solution [3, 4] of fretting fatigue between a cylinder-plane situation. It is also explored how the small fillet at both parts affects the contact as perfectly sharp edges are not physically achievable.

2.2 Boundary conditions

Boundary conditions are given in Figure 2. Face A and Face B are restricted, respectively in x and y directions, consequently, the edge between faces A and B is considered fixed. Two Reference Points are created, being RP1 kinematically coupled to the top and to the sides of the pad, as it is grabbed by the sides. RP2 can only move in direction x and have a kinematic coupling to Face A2 (except during the convergence analysis when A2 and A are defined the same due to no bulk fatigue stress σ_B). These reference points cannot rotate in directions x and y due to symmetry boundary condition and cannot rotate in z direction because the coupling faces are representative of the reduced dimensions of the parts.

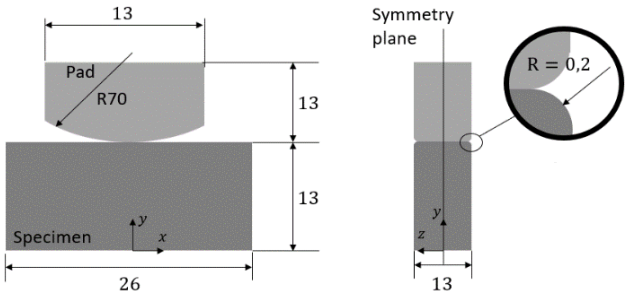

Figure 1: Geometry of the problem, dimensions in mm

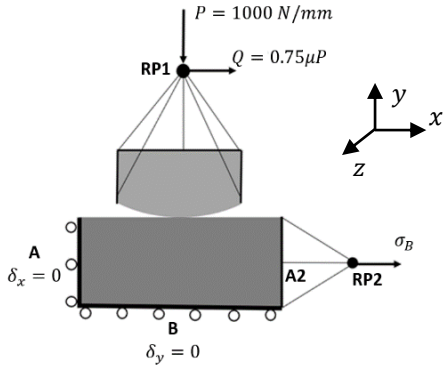

Figure 2: Loads and Boundary conditions

2.3 Contact properties

The contact is imposed as node-to-surface with small sliding formulation, being the pad the primary surface and the specimen the secondary component (master and slave, respectively). For normal contact the Augmented Lagrange method was chosen and for tangential behaviour the Penalty method. The last, a less accurate method, was chosen due to limitations in using symmetry conditions and Lagrange tangential behaviour in ABAQUS. In the penalty method the friction coefficient is defined as μ=0.7.

2.4 Partition, submodel and discretization

As it is a contact problem its necessary to partition the parts for a more refined contact mesh. The near contact mesh will be a rectangular (box in 3D) partition with 3 mm in length and in height that sweeps the whole thickness. The problem will be reduced in half due to a symmetry in the xy plane (can be seen in Figure 1). A symmetric boundary conditions is applied, and all loads are adjusted to half of what a full configuration would be.

Aiming to have all structured hexahedral mesh, the body needs to be divided into 6 faces, so the mesh also

does the same. The region close to the small radius fillet needs to be drawn and swept along the fillet edges as it is shown by the face in Figure 3.

Hence, the partition of the real simulated geometry is presented in Figure 4. The red selected area is the frontal area of the in-contact parts of the partition and will be the submodel. Hence, it was chosen to use a submodel of the contact zone. This helps to decrease the computation time and to link a global and less refined model to a volume representing only the contact region. Again, the red selected surfaces are the frontal area of the submodel in Figure 4.

For the discretization, it was expected to have an element size of 0.1 mm (approximately 130000 total elements) in the submodel region. It is worth noting that representing a precise stress gradient around the fillet is impracticable due to computational reasons. Lastly, the global model will have an approximate element size of 0.4 mm (around 58000 total elements). Both models will be made of hexahedral structured elements for less computational power and better representation of the contact due to less restricted elements. A linear geometric order formulation for the standard solid elements with first order accuracy was considered.

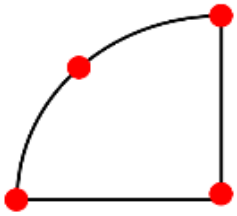

Figure 3: Fillet face partition representation

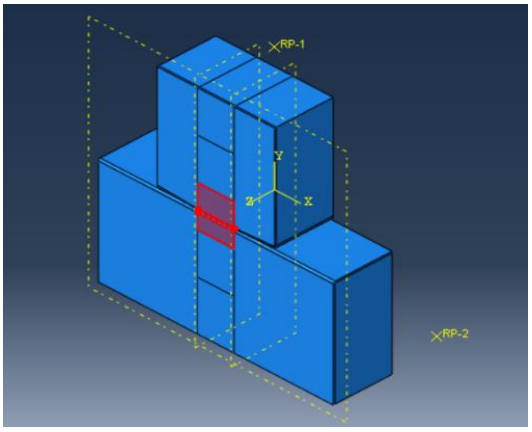

Figure 4: Partition of the fretting assembly

2.5 Material Properties

Simulations will be performed assuming the material as the Aluminium alloy 7075-T651 [7]. The density is $2700\ kg/m^3$, the elasticity modulus is $E = 70\ GPa$ and the Poisson coefficient $\nu = 0.33$. It is worth noting the yield strength is $\sigma_y = 503\ MPa$

2.6 Solution Procedure

The application of forces will be set in steps, first the step for pressure P load and after the fretting Q load step along with the fatigue load of the stress σ_B. All of them are applied in 12 incremental load steps, as depicted in Figure 5. The solution is evaluated at the end of step two when all forces are loaded, and the fretting stress is at maximum.

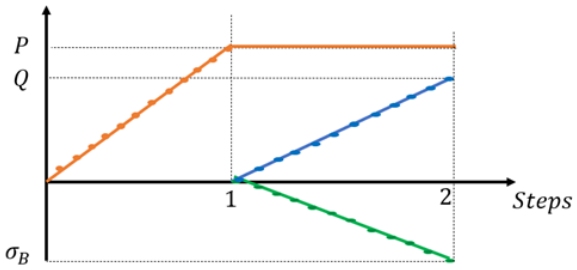

Figure 5: Step load application

3 Convergence and benchmark analysis

This section has the goal to confirm that the 3D model returns representative results when compared with the analytical solution of Cattaneo-Mindlin [3, 4]. The plane-strain state happens in middle plane xy of the model.

The convergence analysis was carried-out with 3 different elements sizes in the submodel. The sizes were 0.20 mm, 0.15 mm, and 0.10 mm. Furthermore, the contact face of the submodel had 21, 28 and 41 elements on its face respectively. The contact pressure and shear stresses were computed respectively in 17, 22 and 31 elements. Figures 6a and 6b shows the contact pressure and the contact shear stress distributions, respectively. Is noticeable that all the results, independent of the mesh sizes selected for this convergence analysis, are converging to a very similar behaviour. Nevertheless, the more refined configuration (mesh size of 0.1) is more capable of highlighting transitions between slip and adhesion zones.

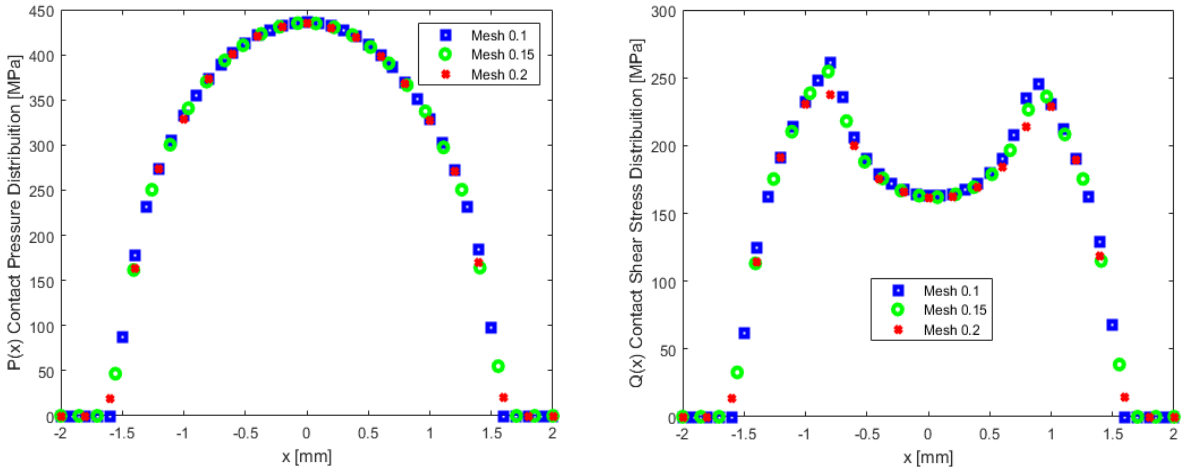

Figure 6: a) Contact Pressure and b) Contact shear stress distribution convergence.

Then, for the benchmark correlation analysis, the results obtained with the element size of 0.10 mm are compared to the analytical solution given by Cattaneo-Mindlin. Figures 7a and 7b show the normal pressure and the shear stress distributions, respectively. A good correlation is observed. The pressure curve falls perfectly over the analytical solution. The shear curve has a small asymmetry in the direction where the fretting load, Q, is applied. One of the reasons for the non-perfect results may be the use of the penalty method in the tangential behaviour of the contact. Nevertheless, the maximum relative error is 3.7% for the contact pressure and for contact shear stress, a very small difference for the purposes of this analysis.

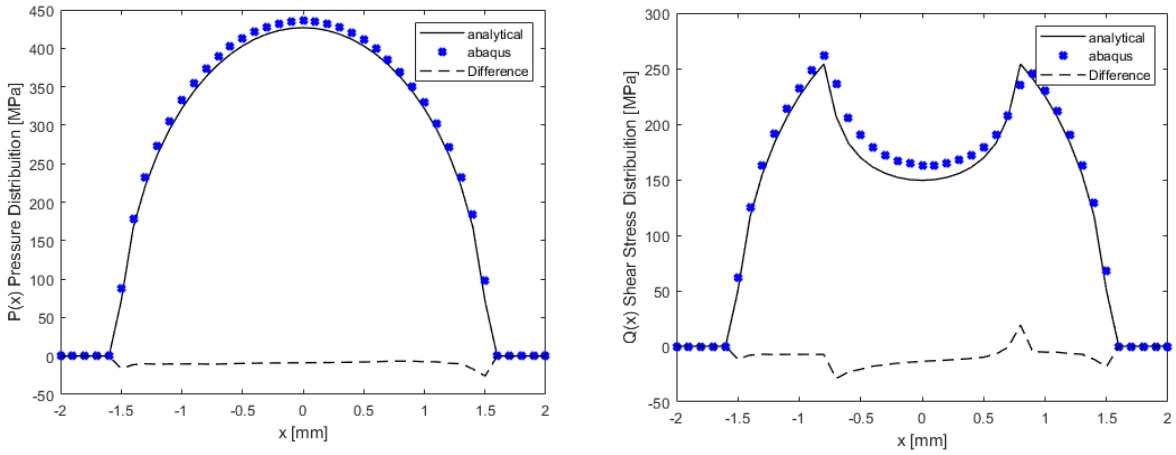

Figure 7: a) Contact Pressure and b) Contact shear stress distribution comparison.

4 Results

In this section, the results are presented for the normal pressure stress and the shear stress. They were retrieved

for the contact stresses in two different ways, one varying stresses along the thickness of the contact (z direction) and other with the stresses varying along the length of the contact (x direction). In the first, the one varying thickness, the contact stresses are computed along the z direction (from $z = 0$ to $z = 6.3mm$) where $x = y = 0$, so its possible to account how much the stresses change along the specimen thickness.

In the second way, the contact stresses are computed along a path varying in normalized x direction from $-a$ to a, in 3 different positions relative to the specimen thickness. One position in the centre ($z = 0$) where the symmetric condition was taken, another position halfway from the centre plane and the outer edge of the contact ($z = 3.2\ mm$), and the last position in the outer edge before the fillet ($z = 6.3\ mm$).

All the simulations were made for 4 different ranges of fatigue load, one without the bulk load $\sigma_B = 0\ N/mm$, one with $\sigma_B = 300\ N/mm$, other with $\sigma_B = 794\ N/mm$ and the last with $\sigma_B = 3077\ N/mm$.

4.1 Normal pressure stress

Firstly, the normal pressure is not affected by the fatigue load as shown Figure 8. This is because the pressure is mostly in the y direction, so a load applied perpendicular to it has little effect. It can be seen in Figure 8 as all plots for different the load cases are overlapping each other.

Additionally, Figure 8 also shows a decrease in normal stress across the specimen's thickness. For better visualization, Figure 9 shows a plot of the contact pressure distribution over the normalized contact semi-length, a. It was chosen to use the results with $\sigma_B = 794\ N/mm$, an intermediary load case since no notable difference would be seen showing all cases.

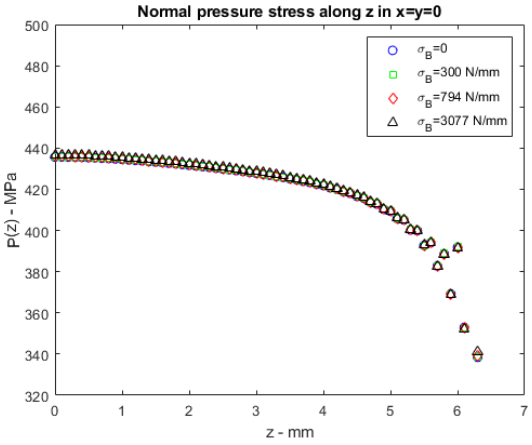

Figure 8: Normal stress distribution along z for different bulk cases

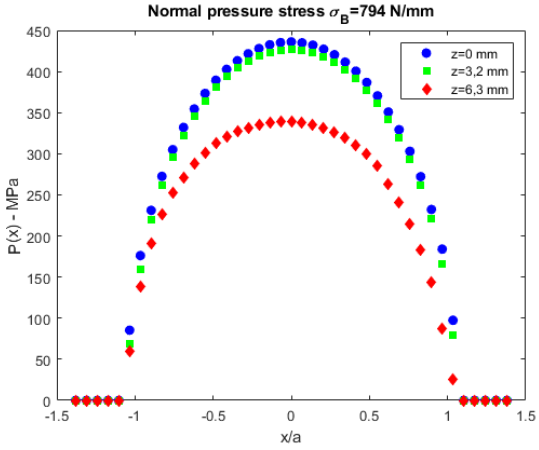

Figure 9: Normal stress distribution along x for different z position

Analysing both Figures 8 and 9 we can see that the pressure decreases more intensely closer to the outer edge. When $z = 3.2\ mm$, the difference between the pressure in the centre ($z = 0$) is small, and it is almost like the analytical 2D solution. However, when analysing the outer edge, $z = 6.3\ mm$, the normal stress can fall to about 23%, which it is not a negligible amount.

4.2 Shear Contact Stress

Figure 10 shows the shear contact distribution along the z axis for all bulk cases. Also, Figures 11a to 11d show the cases along x axis and each one of the four figures represent one bulk case with all three z positions of the thickness ($z = 0; z = 3.2; z = 6.3\ mm$).

From the Figure 10 we can note that the shear contact load increases its base level with the axial load and increase when z is closer to the outer edge $z = 6.3\ mm$. The second statement seems odd because if the pressure decreases close to the edge why would the shear contact increase. The reason for this is the smaller pressure as we can see in Figures 11. The red diamond markers on Figures 11 shows that the base shear stress follows a smaller pressure curve since it is function of it, $q(x) = \mu p(x)$, where it is in the slip zone. The difference is made because when the pressure decreases the stick zone also decreases in size, showing a smaller gradient and consequently a higher value compared with the centre of the shear stress in the centre and halfway.

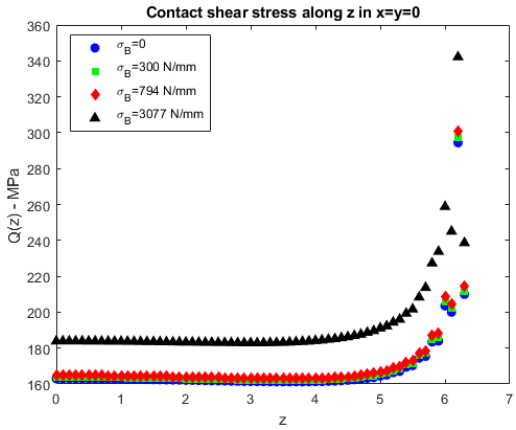

Figure 10: Shear stress distribution along z for different bulk cases

Another reason is related to the bulk load. The bulk load tends to displace the stick zone in its direction and because of that, the z path ($x = y = 0$) does not coincide with the centre and a it gives lower value for the shear stress.

With all that said, it is interesting to know what effect this decentralized high shear effort can mean in an equivalent stress parameter when analysing the whole component. Figure 12 shows an image of the submodel part of the specimen highlighting where the contact is with the stress presented in terms of Tresca Equivalent stress (2 times the maximum shear stress). This image again is from the simulation where the bulk load is $\sigma_B = 794\ N/mm$.

On the Figure 12 is possible to see a concentrated stress of 624 MPa near the border edge in the vicinity of the considered milling fillet. Metallic materials often nucleate cracks due to shear stress and this accumulated stress can be one of the reasons why this type of specimen is so sensible to alignment and seldom presents border cracks, which are undesirable and not possible to compute when considering only the 2D analysis for the stresses and they invalidate the test specimen. Lastly, the load configuration with $\sigma_B = 794\ N/mm$ is over the yield strength of the material, and it is true that the analysis of the case as well as the one with $\sigma_B = 3077\ N/mm$ do not represent perfectly the material phenomenon since it will be outside the elastic behaviour. Nonetheless, it represents well the trend for the specimen's edge concentration stress when the behaviour is elastic.

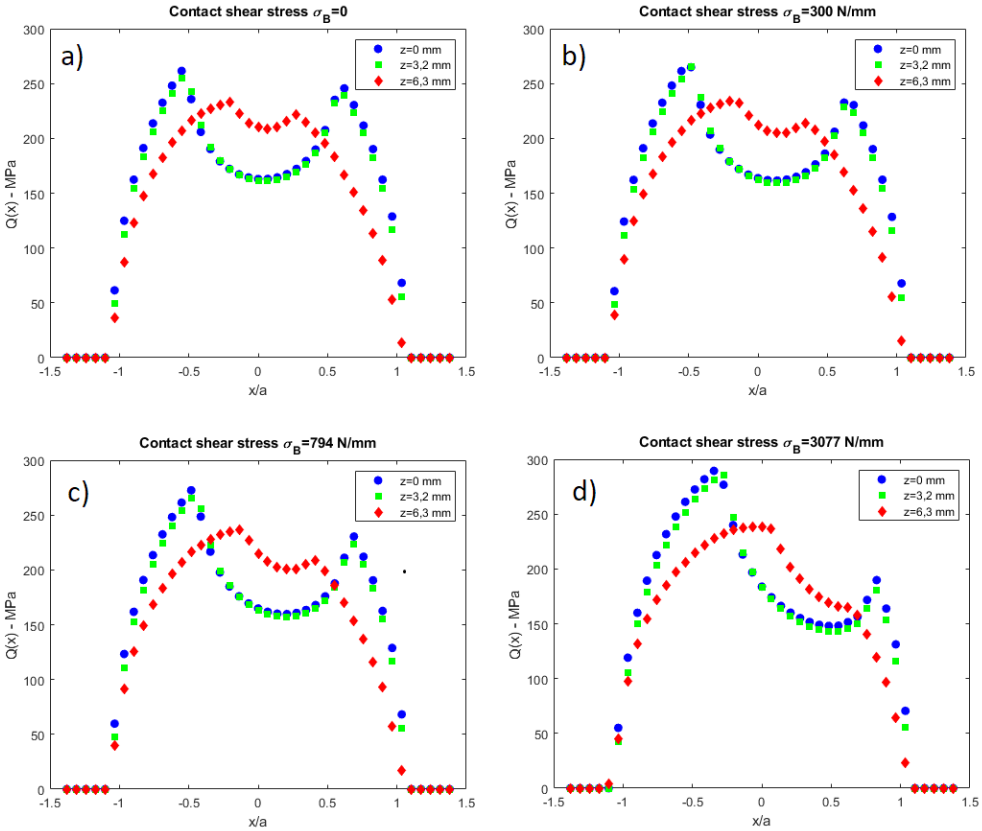

Figure 11: Shear stress distribution along x for different bulk. a) $\sigma_B = 0$; b) $\sigma_B = 300\ N/mm$; c) $\sigma_B = 794\ N/mm$; d) $\sigma_B = 3077\ N/mm$.

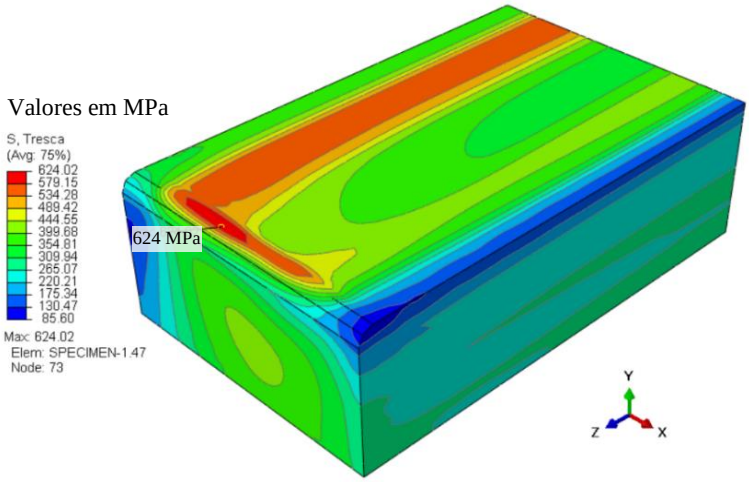

Figure 12: Tresca stress distribution when $\sigma_B = 794\ N/mm$.

5 Conclusions

A comparative analysis of the contact pressure and shear stress when employing either a 3D numerical approach or a 2D plane-strain approach for the modelling of a cylinder-to-flat fretting configuration, including fatigue bulk load, has been presented. The analysis has been carried-out using a popular fretting specimen-pad configuration, where both have the same thickness and there are small fillets on their edges, which are representative of the milling fabrication process. It is clear from the results that although the 2D analysis can be simpler and return representative results, fretting fatigue load produces a non-negligible difference when employing a 3D model. The 3D analysis is able to return different estimates of stress on the edges of the fretting fatigue specimens and even explain some undesired test failures, as example of cracks that nucleates on the edges and not in the centre of the specimen.

Future works aim to compute fatigue parameters (such as Smith-Watson-Topper and Fatemi-Socie) and link them to life estimates and further improve the knowledge of the fretting fatigue 3D configuration.

Acknowledgements. The authors would like to thank and acknowledge the Brazilian Public Organizations FAPDF and CNPq for their Support.

Authorship statement. The authors hereby confirm that they are the sole liable persons responsible for the authorship of this work, and that all material that has been herein included as part of the present paper is either the property (and authorship) of the authors or has the permission of the owners to be included here.

References

[1] D.A. Hills, D. Nowell, Mechanics of Fretting Fatigue, Kluber Academic Publishers, Dordrech/Boston/London, ISBN: 0-7923-2866-3, 1994.
[2] R.B. Waterhouse, Fretting Fatigue, Applied Science Publisher, London, ISBN: 0-8529-8940-7, 1981.
[3] Mindlin, Raymond David. "Compliance of elastic bodies in contact." (1949): 259-268.
[4] Cattaneo, C. "Sul contatto di due corpi elastici: Distribuzion local degli sforzi Reconditi dell Accademia nazionale dei Lincei, 1938, 27, 342–248, 434–436, 474–478." Google Scholar.
[5] Araújo J, Nowell D. The effect of rapidly varying contact stress fields on fretting fatigue. Int J Fatigue 2002;24:763–75.
[6] Nowell D, Dini D, Hill DA. Recent developments in the understanding of fretting fatigue. Eng Fract Mech 2006;73:207–22.
[7] Rangel, D., Erena, D., Vázquez, J., & Araújo, J. A. (2022). Prediction of initiation and total life in fretting fatigue considering kinked cracks. Theoretical and Applied Fracture Mechanics, 119, 103345.
[8] J. Vázquez, C. Navarro, J. Domínguez, Two dimensional versus three dimensional modelling in fretting fatigue life prediction, J. Strain. Anal. Eng. Des. 51 (2016) 109–117, http://dx.doi.org/10.1177/0309324715611510.A
[9] Vázquez, J., et al. "3D contact effects in fretting fatigue tests." Theoretical and Applied Fracture Mechanics 118 (2022): 103260